iScience

CellPress
OPEN ACCESS

Article

Composite electrolyte used for low temperature SOFCs to work at 390°C

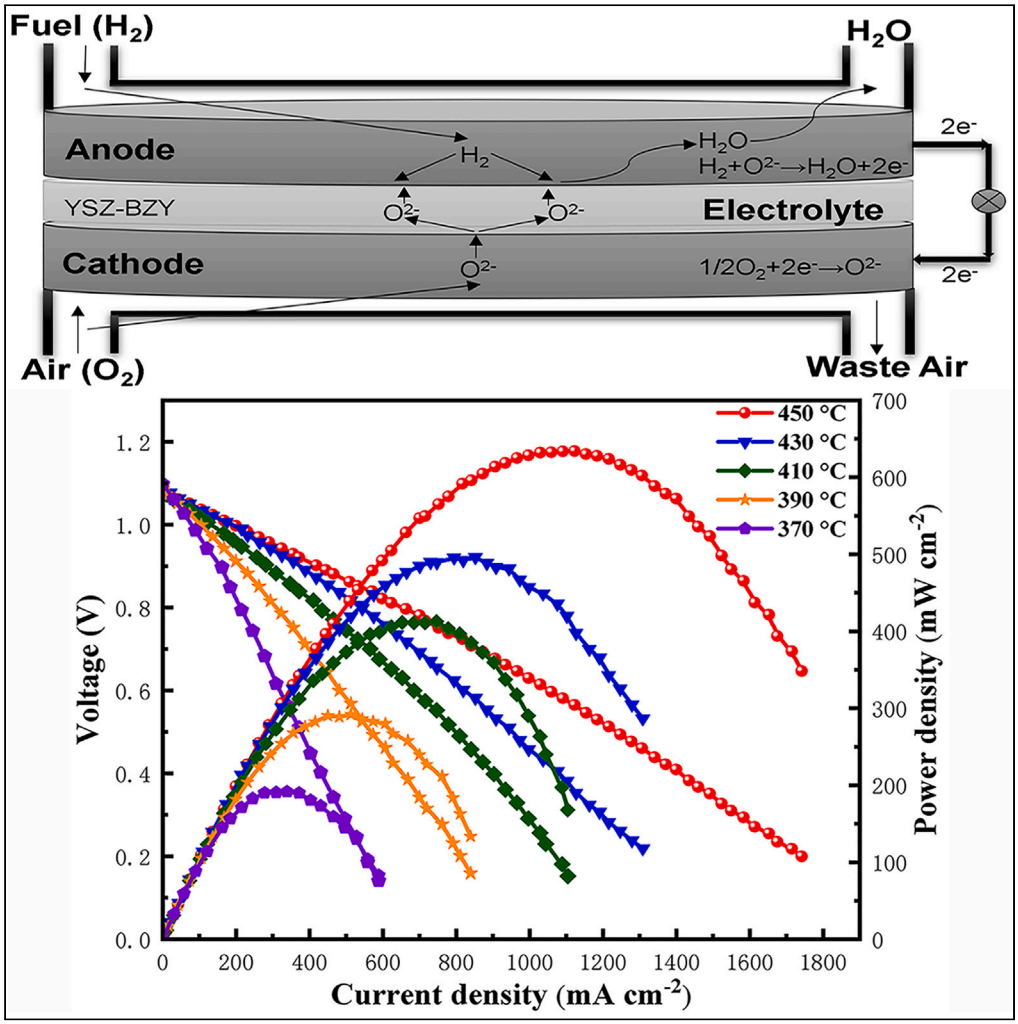

Yu Liu, Liwen Zuo, Cong Jiang, Dan Zheng, Baoyuan Wang

zhengdanwby@163.com (D.Z.)
baoyuanw@163.com (B.W.)

Highlights

A novel composite electrolyte was fabricated on line

Excellent performance below 400°C, 634 mW cm^{-2} at 450°C and 200 mW cm^{-2} at 370°C

In situ formation of amorphous $BaCO_3$ is conducive to interface conduction

The proton conduction activation energy of the YSZ-BZY composite is 0.41eV

Liu et al., iScience *26*, 107002
July 21, 2023
https://doi.org/10.1016/j.isci.2023.107002

iScience

CellPress
OPEN ACCESS

Article

Composite electrolyte used for low temperature SOFCs to work at 390°C

Yu Liu,[1,2] Liwen Zuo,[2] Cong Jiang,[2] Dan Zheng,[1,*] and Baoyuan Wang[2,3,*]

SUMMARY

A combination of yttria stabilized zirconia (YSZ) and $Ba(NO_3)_2$ commercial powders was used as electrolytes in the construction of symmetrical SOFC. As X-ray diffraction pattern and Raman spectra revealed, the YSZ-$Ba(NO_3)_2$ electrolyte *in situ* converted into YSZ and yttrium-doped barium zirconate (BZY) composite at 450°C in hydrogen atmosphere. The power maximum (P_{max}) of YSZ-BZY based fuel cell can reach 634.06 mW cm^{-2} at 450°C. Notly, the P_{max} can evenly maintain at 300 mW cm^{-2} as the operational temperature reduced to 390°C. The outstanding cell performance at low temperature indicate the excellent ion conductivity of the composite electrolyte. The promising ion conductivity is originated from the proton conduction of BZY, the oxygen conductivity of YSZ, and the enhanced ion conduction through interface transport. Our work demonstrates that the developed YSZ-BZY electrolyte holds enormous potential for LT-SOFCs.

INTRODUCTION

Solid oxide fuel cells (SOFC) can transform chemical energy of fuel directly into electrical energy without fierce burning, and it have been acknowledged as one of the most promising green energy devices for the 21st century because of its unique advantages including high conversion efficiency, low environmental impact and fuel diversity, thus they have a lot of potential in fulfilling the growing energy demand and environmental sustainability needs.[1–3] Yttria stabilized zirconia (YSZ) is considered as the most successful electrolyte material to date because of its outstanding chemical stability, thermal stability and mechanical strength under fuel cell conditions.[4–6] The main disadvantage of the YSZ electrolyte is that its working temperature is excessively high (>800°C), which is required for YSZ to achieve adequate oxygen ion conductivity and to further achieve decent cell performance. High operating temperatures cause sealing issues and thermal expansion mismatches between fuel cell components, thus impeding the commercialization of YSZ-based SOFCs.[7,8] As a result, lowering the operating temperature of SOFCs to below 600°C is a critical technical pathway in the future to reduce manufacturing material costs and long-term durability.[9,10] In general, there are two ways to reduce the operating temperature of SOFC, one is to reduce the thickness of the electrolyte film, but this method is limited by the complexity of the equipment. Another approach is to find new electrolyte materials to replace YSZ. Low temperature electrolytes put forward higher requirements, it must have high ionic conductivity and low electronic conductivity in the low temperature range, but also need to have good contact with the electrode at the working temperature to ensure that will not produce shedding and peeling.[11–13] It was reported that the new electrolyte materials such as samarium-doped ceria (SDC), gadolinium -doped cerium oxide (GDC) and strontium-and magnesium-doped lanthanum gallate (LSGM), et al.[14–17] possess higher ionic conductivity at intermediate temperatures in comparison with YSZ, but their ion conductivity is insufficient at low temperature to support promising power output. In addition, various of composites were exploited for the electrolyte application of low-temperature SOFC, Table 1[18–25] listed composite electrolytes developed in recent years that can work in low temperature range, the corresponding cell performance and ionic conductivity collected. It can be seen from the table that several electrolytes can still work normally at about 450°C, but few electrolytes were reported to support the cell performance below 400°C. Exploiting electrolyte that can deliver excellent power output at 450°C and can normally work below 400°C should simplify the preparation process and significantly reduce the cost.

In this work, a new type of yttria stabilized zirconia and yttrium-doped barium zirconate (YSZ-BZY) composite electrolyte is successfully demonstrated to work at a low temperature of 390°C, which was motivated by

[1]School of Electronic Engineering, Wuhan Vocational College of Software and Engineering, Wuhan, Hubei, PR China

[2]School of Microelectronics, Hubei University, Wuhan, Hubei 430062, PR China

[3]Lead contact

*Correspondence: zhengdanwby@163.com (D.Z.), baoyuanw@163.com (B.W.)

https://doi.org/10.1016/j.isci.2023.107002

Table 1. Electrolytes that can work at low temperature have been reported in recent years

Electrolyte	Working temperature (°C)	Fuel cell performance (mW/cm^2)	Ionic conductivity (S/cm)
SCDC-NCAL[18]	500	460	
	450	400	
	400	360	
SDC-$LSCO_4$[19]	450	386	
SDC-SSC[20]	500	500	0.155
	475	367	0.114
$LiNiO_2$-GDC[21]	500	350	
	450	300	
	400	250	
BCFZY-ZnO[22]	500	479	0.260
	450	300	
	400	189	0.110
SDC-$Li_{0.5}ZnO$[23]	500	450	
	480	401	
Hematite−LCP[24]	500	490	
	450	386	
LCP-ZnO[25]	500	500	
	475	300	

the ideas presented above. The composite material is sandwiched in the middle with two Ni-NCAL ($Ni_{0.8}Co_{0.15}Al_{0.05}LiO_{2-\delta}$) electrodes to assemble a symmetrical fuel cell. Various characterizations have been used to systematically study the fuel cell's properties. The findings demonstrate the enormous potential of YSZ-BZY composite electrolyte for low-temperature SOFC.

RESULTS AND DISCUSSION

Figure 1 presented the SEM images of the as-prepared YSZ, $Ba(NO_3)_2$ and YSZ-$Ba(NO_3)_2$ powders. As Figure 1A shown, the particle size of commercial YSZ ranges from hundreds of nm to several μm with irregular shape, obviously its morphological features are uneven because of lack of precise control on the size and morphology of the commercial YSZ powder. Figure 1B depicted that the commercial $Ba(NO_3)_2$ aggregated as lots of blocks. Figures 1C and 1D expressed the morphology of YSZ-$Ba(NO_3)_2$ composite powder in a 50:50 mass ratio. It can be observed that the composite powder were in its natural state, the YSZ particles adhered on the surface of a large $Ba(NO_3)_2$ bulk.

To assess the potential of YSZ-$Ba(NO_3)_2$ composite electrolyte, the density-voltage (I-V) and current density-power (I-P) curves of YSZ-$Ba(NO_3)_2$ based fuel cells were evaluated. In this study, four cells were prepared according to different mass ratios of YSZ to $Ba(NO_3)_2$ (45:55 for cell 1, 50:50 for cell 2, 55:45 for cell 3, 60:40 for cell 4. Figure 2A depicts the electrochemical performance of the four cells using H_2 as fuel and air as an oxidant at 550°C. Obviously, the composition of electrolytes significantly influences the electrochemical performance of assembled cell. The power maximum (P_{max}) initially enhanced with the increase of $Ba(NO_3)_2$ content, and then decrease as the $Ba(NO_3)_2$ content further increased to 60 wt %. When the mass ratio of YSZ to $Ba(NO_3)_2$ is 50:50 (cell 2), the highest power density of 792.5 mW cm^{-2} with open-circuit voltage of 1.006 V were achieved at 550°C. Moreover, the cell 2 with optimum mass ratio underwent the low-temperature potential tests as Figure 2B shown, it was discovered that the cell 2 delivered exciting electrochemical performance in low temperature range, 634.063 mW cm^{-2} at 450°C, 500 mW cm^{-2} at 430°C, 420 mW cm^{-2} at 410°C and 300 mW cm^{-2} at 390°C. Evenly the P_{max} can maintain at 200 mW cm^{-2} as the operational temperature reduced to 370°C.

The unexpected cell performance at low temperature indicated that the composite developed in this work has enormous advantage in electrolyte application for low temperature SOFC. EIS characterization was carried out to peer the electrochemical process of the cell 2. Figure 2C displays the EIS results in the

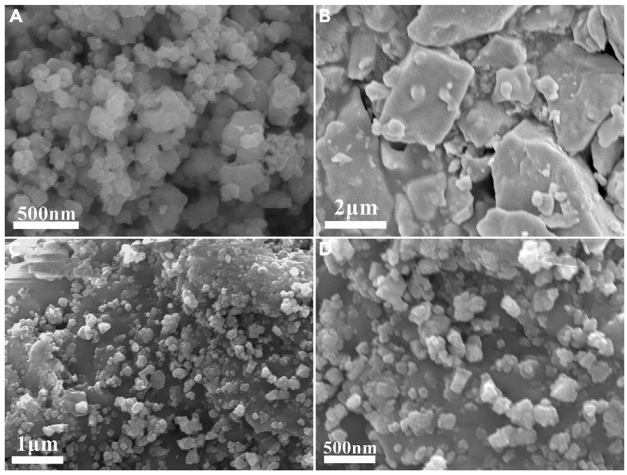

Figure 1. SEM images of materials

(A–D) SEM images of commercial YSZ (A), commercial $Ba(NO_3)_2$ (B) and the as-prepared YSZ-$Ba(NO_3)_2$ composite with mass ratio of 1:1 (C, D).

temperature range of 450-370°C, and the inset presented the equivalent circuit of $R_0//R_1Q_1//R_2Q_2$ using for simulation. Table 2 lists the fitting parameters through simulating, wherein Q is a non-ideal capacitor known as a constant phase element (CPE). The Ohm resistance (R_0) is made up of the ion conduction resistance in the electrolyte as well as the electron transfer resistance in the electrode. R_0 usually equal to the first intersection of the real axis (X axis) at high-frequency semicircle.[26] R_1 is designated as the interface resistance, namely the ion transfer resistance from the electrode to the electrolyte, corresponding to the first arc at intermediate frequency. R_2 is the low-frequency arc that represents the mass transfer including gas adsorption and desorption.[27] The sum of R_1 and R_2 was defined as the electrode polarization resistance (R_p).[28] Because the increase of temperature should accelerate the electron migration in the electrode and the ion transport in the electrolyte, the ohmic resistance R_0 decreases with temperature rises as shown. In addition, when the temperature increases from 370 to 450°C, the Rp decreases from 0.999 Ω cm^2 to 0.212 Ω cm^2. It is significant to note that the lowest polarization resistance is just 0.212 Ω cm^2 at 450°C, demonstrating the excellent catalytical activity of NCAL electrode at low temperature.

Figure 3A showed the XRD pattern of cell 2 electrolyte powder scratch from the tested cell, which was operated in H_2/air atmosphere at 450°C for 1h. The diffraction peaks located at 30.1°, 34.9°, 50.1°, 59.6° and 73.6° can be indexed to (1 0 1), (0 0 2), (1 1 2), (1 0 3) and (0 0 4) planes of fluorite YSZ (JCPDS NO. 82–1244) , these peaks at 21.1°, 30°, 36.9°, 42.9°, 53.2°, 62.3° and 70.7° corresponded to the (2 0 0), (2 2 0), (2 2 2), (4 0 0), (4 2 2), (4 4 0) and (6 2 0) planes of perovskite BZY in according to our previous report,[29] indicating that the YSZ-$Ba(NO_3)_2$ (50:50) composite powder is no longer the original composite material. In H_2 atmosphere, the two-phase composite material is unstable, YSZ have on-line reacted with portion of $Ba(NO_3)_2$ to produce yttrium-doped barium zirconate (BZY), which is subsequently recombined with YSZ. Thus the YSZ-$Ba(NO_3)_2$ electrolyte should converted into YSZ-BZY electrolyte during the pre-treated by H_2. As experimental section described, all the cells must be pre-treated by H_2 for 1h before performance testing to make sure that the conversion of YSZ-$Ba(NO_3)_2$ to YSZ-BZY have been finished.

Figure 3B displays the typical Raman spectrum of the tested YSZ-BZY electrolyte. The Raman features primarily originate from vibration modes, the lattice disorder may be exacerbated as a result of mutual diffusion between the two levels. The Raman peaks roughly at 465 cm^{-1} and 718 cm^{-1} equivalent to the vibration mode of BZY,[30–32] and the Raman peak at approximately 623 cm^{-1} is indexed to YSZ,[33,34] respectively. According to the literature, the CO_3^{2-} ion is known to produce two distinct internal vibration motions: (1) a ν_4 correlation band, which is produced by the CO_3^{2-} group's symmetric in-plane bending vibration, corresponding to the peak at 692 cm^{-1} in $BaCO_3$, (2) a ν_1 related band, which is generated by CO_3^{2-} group symmetric tensile vibrations, occurring the peak at 1058 cm^{-1}.[35–37] As Figure 3B shown, peaks at 690 cm^{-1} and 1059 cm^{-1} does not belong to YSZ or BZY, and it is speculated to be the $BaCO_3$ substance. Since the XRD patterns of YSZ-BZY pellet does not present any diffraction peak concerning with $BaCO_3$, thus the form of $BaCO_3$ actually exists as amorphous state.

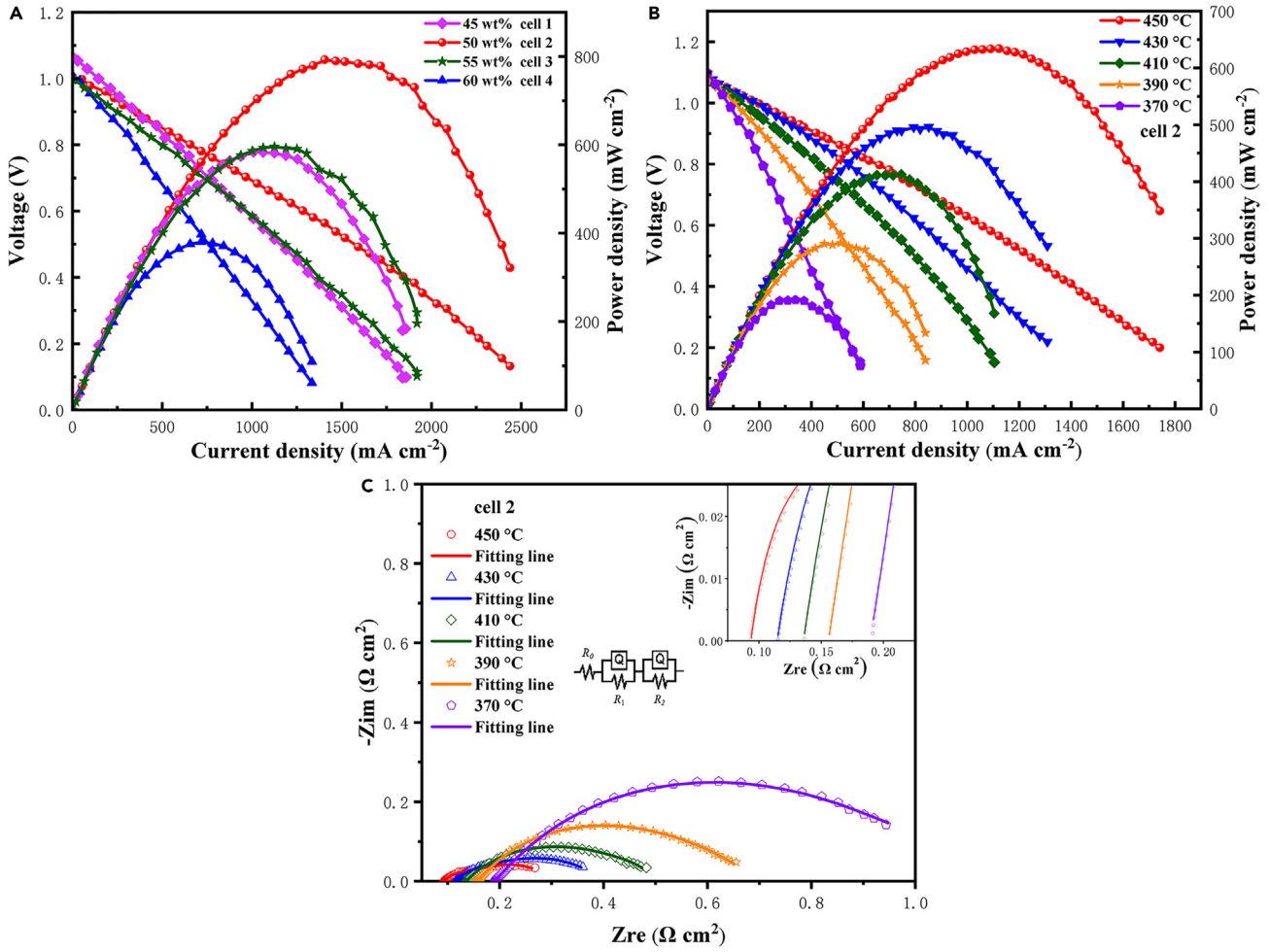

Figure 2. Performance test and electrochemical characterization

(A–C) I-V and I-P characteristics of the four cells with different composition at 550°C, (B) electrochemical performance and EIS result (C) of cell 2 measured at 450°C–370°C.

The cross-sectional SEM of symmetrical Ni-NCAL/YSZ-BZY/Ni-NCAL cells after performance testing in H_2/Air at 450°C is shown in Figure 4A. A three-layer structure was clearly distinguished, the middle layer should be the YSZ-BZY electrolyte with a thickness of roughly 700 μm. No cracks were observed in the interface area, the YSZ-BZY electrolyte membrane close contact with the Ni-NCAL electrodes on both sides, indicating that the YSZ-BZY composite have compatible thermal expansion coefficient with that of NCAL electrode. The magnified SEM image of the electrolyte is shown in Figure 4B. The YSZ-BZY electrolyte used in this case is unlike the normal high-temperature sintered electrolyte because it is consisted of abundant particles without typical grain boundaries. However, the particles are tightly packed together, there aren't any obvious continuous pores or penetrating cracks. Thus, the YSZ-BZY electrolyte is likewise thought to be airtight as has been noted in other papers.[38] The detailed morphology of cathode and anode are depicted in Figures 4C and 4D, respectively. The porous nature of the NCAL electrode makes it easier for air or H_2 to diffuse through it. In addition, after performance testing the anode exhibited significantly different morphology compared with cathode. The NCAL on cathode side presented as micrometer sphere, which was composed by lots of small particles it is visible that the NCAL sphere of the anode are obliterated by H_2.

Figures 4E–4K show the element mapping of the tested fuel cell from a cross-sectional view. The uniform distribution of Ba, Zr, Y and O elements in the interlayer confirms the existence of BaZrY-oxide in the electrolyte membrane. In addition, no nitrogen element was detected in the electrolyte membrane, which is well consistent with XRD results, proving that the YSZ-$Ba(NO_3)_2$ electrolyte have converted into YSZ-BZY after H_2 treating

Table 2. The EIS fitting results

T (°C)	R_0	Q_1	n_1	R_1	Q_2	n_2	R_2	R_p	ASR
450	0.0935	0.5012	0.6667	0.0492	3.0180	0.5742	0.1627	0.2119	0.1356
430	0.1148	0.5895	0.6351	0.0618	1.6350	0.5640	0.2202	0.2820	0.1804
410	0.1359	9.0640	0.6847	0.0644	0.3559	0.6133	0.3039	0.3683	0.2357
390	0.1558	0.2588	0.7855	0.1825	0.6333	0.5524	0.3548	0.5373	0.3439
370	0.1888	1.8700	0.4412	0.3882	0.1575	0.7303	0.6109	0.9991	0.6394

NCAL was used as the electrode material, which is responsible for the uniform distribution of Ni, Co, and Al in the bilateral layers. In addition, the cathode region has a larger O element content than the anode region. The discrepancy in O element distribution results from the reduction of NCAL on the anode region. Owing to the sensitivity restrictions of EDS detectors, the tiny atomic mass of Li is too light to be detected.

TEM was used to observe the further microstructure of the tested YSZ-BZY electrolyte, which were ground into powder and dispersed in ethanol through ultrasonic treatment. The samples were then dropped onto a lacey carbon TEM grid and dried in the air to complete the sample preparation for TEM characterization. A low-resolution TEM picture of the tested YSZ-BZY electrolyte is shown in Figures 5A and 5F. The electrolyte particles exhibit fuzzy grain boundaries with a wide size distribution. Figures 5B–5E depicts the associated TEM-EDS mapping image. Different elements were represented by different colors. As XRD result presented, the tested YSZ-$Ba(NO_3)_2$ have converted into YSZ-BZY composite, thus Ba element located in the lower right corner should correspond to the BZY phase, and the YSZ component situated in the upper left region. Both of BZY and YSZ phases possessed Zr and Y element, thus Zr, and Y are evenly dispersed through all the area. The mapping of oxygen components in the image allows us to deduce that all metal elements are in the oxidation state. More importantly, the interface regions between YSZ and BZY particles are numerous and tightly related to the two-phase materials over the overlapping region, which can offer ion conduction pathways to improve ion conductivity.[39] A normal charge transfer route for oxygen ion conduction is also established during the YSZ phase, which is crucial for cell performance.

The HR-TEM images of the tested YSZ-BZY electrolyte are displayed in Figures 5G and 5H. The lattice fringes with lattice space of 0.2096 nm and 0.2477 nm corresponded to the (2 0 0) and (1 1 1) crystal planes of perovskite BZY, respectively. The (1 0 1) and (1 0 2) crystal planes of fluorite YSZ are represented by lattice fringes with lattices spacings of 0.2971 nm and 0.2169 nm, respectively. It is possible to clearly see the interface between BZY and YSZ. In the YSZ-BZY composites, these numbers of interfaces help to increase ionic conductivity by interfacial conduction. In addition to crystal particles with obvious lattice fringes (h), amorphous materials (shown by white arrows) without lattice fringe can be seen surrounding crystal particles in Figures 5G and 5H. It is assumed that the amorphous substance is $BaCO_3$, which was generated *in situ* with BZY during the performance testing and is quite compatible with the Raman characterization. The amorphous $BaCO_3$ is produced in the fuel cell operating environment by a sequence of reactions that take place inside the fuel cell, part of $Ba(NO_3)_2$ reacted with YSZ to produce BZY, whereas the other part of $Ba(NO_3)_2$ reacts with H_2O produced during the test to form $Ba(OH)_2$. Finally, $Ba(OH)_2$ reacts with CO_2 in the air to produce $BaCO_3$.

To peer the underlying reason for the exciting electrochemical performance of YSZ-BZY electrolyte at low temperature, the conductivity of the tested YSZ-BZY electrolyte were characterized in different atmosphere. YSZ-BZY powder was compressed under a loading of 500 MPa to obtain cylinder pellets, which were brushed by Pt paste for ionic conductivity test or Ag paste for electronic conductivity test. Then linear scan voltage (LSV) method was adopted to characterize the electrical conductivity at different temperature. In detailed, the swept voltage of -1V–1V was applied on both sides of these pellets and the response current were recorded by digital source instrument (Keithley 2460), the resistance was calculated from the slope of the I-V curves, and then converted into electrical conductivity under the consideration of pellet dimension. The relationship between electrical conductivity and temperature can be described by a thermally activated Arrhenius equation and expressed as:

$$\ln(\sigma T) = \ln A - \frac{E_a}{kT} \quad \text{(Equation 1)}$$

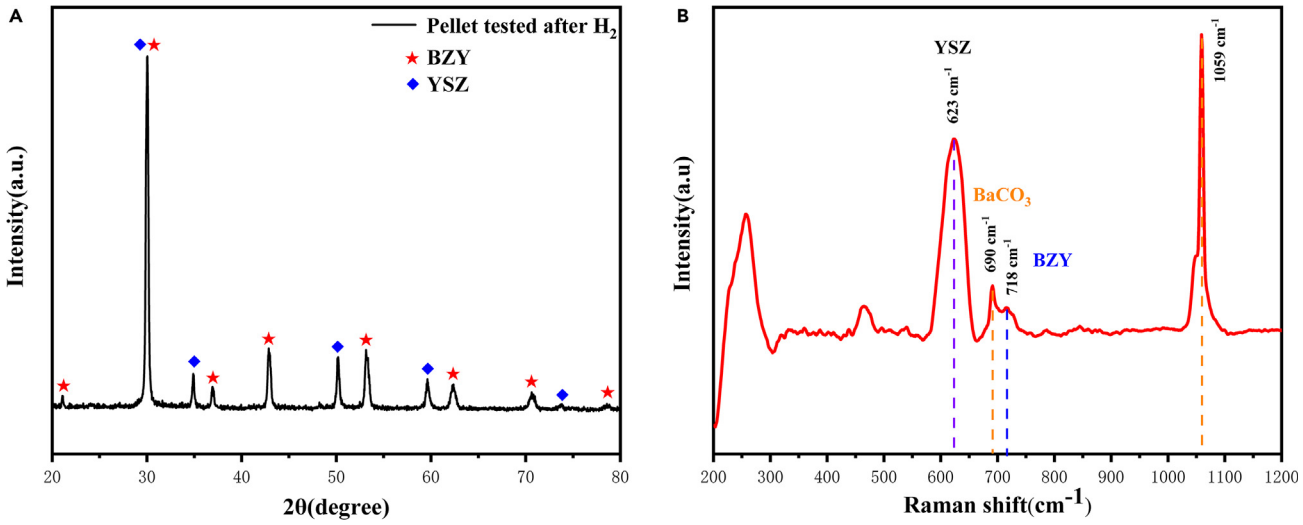

Figure 3. XRD and Raman characterization

(A and B) The XRD patterns (A) and Raman spectrum (B) of YSZ-BZY electrolyte powder scratch from the cell tested at 450°C for 1h.

where A is the pre-exponential factor, T represented the absolute temperature, k is the Boltzmann constant, and E_a is the activation energy for conduction. In order to obtain the Ea, the relation of electrical conductivity and temperature was converted into the relation of ln(σT) to 1/T, which were successfully fitted by line. The activation energy for electrical conductivity was subsequently obtained from the slope of the plot of ln(σT) versus the reciprocal of the absolute temperature. The proton conductivity obtained in hydrogen atmosphere as a function of temperature was expressed in Figure 6A The activation energy of proton motion in the tested YSZ-BZY electrolyte is found to be 0.41 eV at 400–500°C according to the Arrhenius curve, indicating that within this temperature range, the energy needed for proton transport from its normal state to an active state where chemical reactions are likely to occur is relatively low, thus proton transport is easier compared with oxygen ion conduction. Figure 6B gives the Arrhenius curve of the tested YSZ-BZY electrolyte obtained in air atmosphere; it can be inferred that the composite material has a relatively low oxygen ionic conductivity at low temperatures. This is because of the fact that the poor oxygen ionic conductivity of pure BZY inhibits oxygen ions from going through the cell interior. The proton conductivity of the tested YSZ-BZY is almost an order of magnitude higher than oxygen ionic conductivity, namely the electrolyte membrane was dominated by proton conductivity, which facilitate the outstanding low temperature performance. As Figure 6C shown, the electronic conductivity obtained in N_2 environment is relatively low in the 400–500°C temperature range, suggesting that the transmission of electrons is almost impeded by the electrolyte membrane, which is more favorable for cell performance.

XPS characterization was used to examine the revolution of elemental valence state after performance testing. Figure 7 compared the XPS O 1s obtained from the pure YSZ and the tested YSZ-BZY electrolyte. Deconvolution of the spectrum yields a number of peaks that correspond to various symmetric signals. The spectrum can be deconvoluted into several peaks, the peak centered at approximately 529 eV is attributed to the lattice oxygen (O_L), and the O-H bond of the adsorbed water molecules and the existence of oxygen defects are credited with the peak located at approximately 531 eV, which compensates for the defects of metal oxides and is related to oxygen vacancies (O_V), the peak located at 533 eV is attributed to the absorption oxygen species (O_A).[40] It has been noted that the content of the oxygen vacancy in pure YSZ is calculated to be 43% in Figure 7A, and BZY is reported to be 55%,[38,41,42] whereas for the tested YSZ-BZY electrolyte the oxygen vacancy content deduced from the area ratio of peaks is 80%, the oxygen vacancy are already present on the surface of the initial untested powder, and the concentration of oxygen vacancy is greatly increased after testing under fuel cell conditions. This suggests that additional oxygen vacancies will be produced in the electrolyte on-site when the cell is operating. However, the newly formed oxygen vacancy in the tested YSZ-BZY electrolyte plays a significant role in enhancing ionic conductivity for superior cell performance.

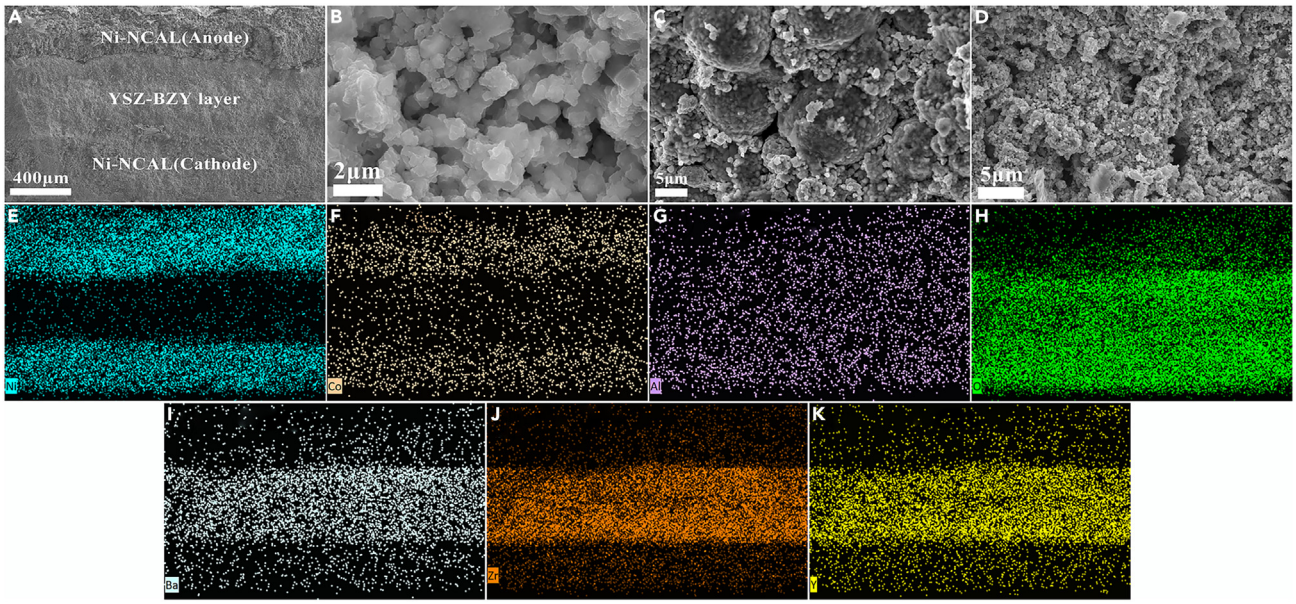

Figure 4. Cross-sectional SEM images and EDS mapping images

(A–K) Cross-sectional SEM images of the tested YSZ-BZY fuel cell, (B) Detailed morphology of the YSZ-BZY electrolyte membrane, (C) Magnified SEM images of cathode region (C) and anode region (D), (E–K) EDS mapping of the tested fuel cell from the cross-sectional view.

Furthermore, Figure 8 shows the stability of the electrolyte layer evaluated under a stationary current density of 100 mA cm^{-2} at 450°C. The cell working voltage was maintained at around 0.85 V for 30 h without any significant degradation. The experimental results show that the overall stability is more than 30 h at 450°C, which is not common in the low temperature environment of 450°C reported previously.

Conclusion

The cell fabricated from YSZ-BZY electrolyte delivered P_{max} of 634.06 mW cm^{-2} at 450°C, and evenly maintained at 300 mW cm^{-2} as the operational temperature reduced to 390°C, the decent cell performance demonstrates the YSZ-BZY electrolyte composite electrolyte can normally work at near 400°C, which has

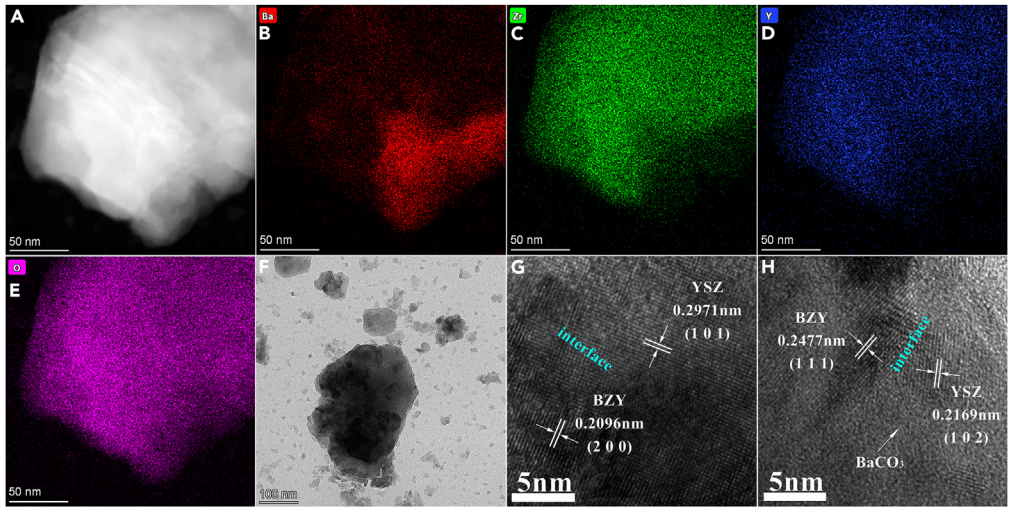

Figure 5. TEM and HR-TEM images of the tested YSZ-BZY electrolyte

(A–H) Low-resolution TEM image (A, F), TEM-EDS mapping images (B–E) and HR-TEM images (G, H) of the tested YSZ-BZY electrolyte.

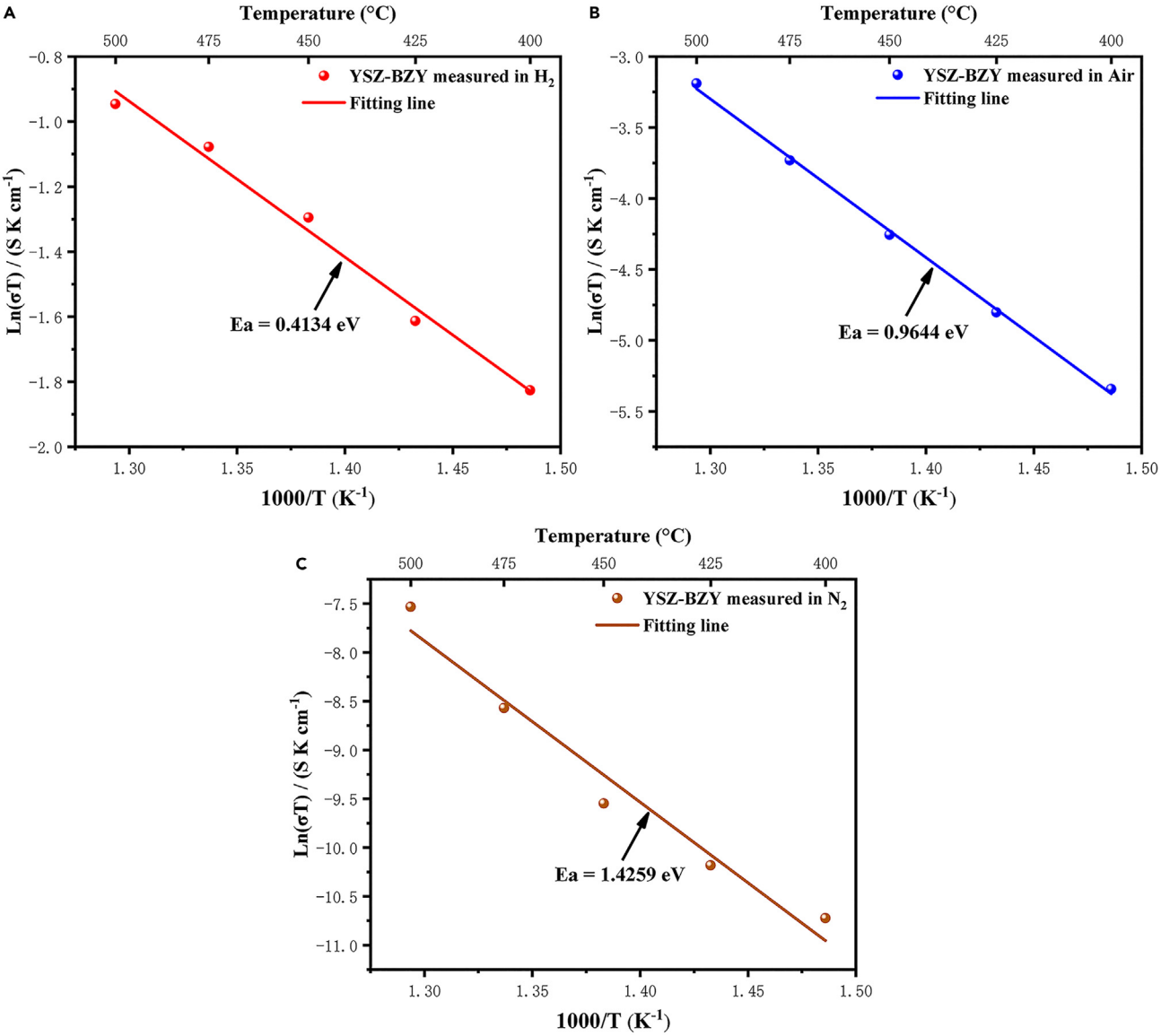

Figure 6. Arrhenius curves analysis

(A–C) Arrhenius curves of the tested YSZ-BZY electrolyte obtained in different atmosphere: in H_2 (A), in air (B), in N_2 (C).

been rarely reported in literature. XRD result revealed that the YSZ-$Ba(NO_3)_2$ composite material was on-line converted into BZY and YSZ composite in hydrogen atmosphere at 450°C. As XPS characterization shown, the oxygen vacancies of the composite electrolyte material are significantly higher than the previously reported pure BZY and YSZ. The newly created oxygen vacancies enhance ionic conductivity for greater cells performance. Raman and TEM characterization anticipate the presence of amorphous $BaCO_3$ in the composite, and the interface formed in the composite helped to improve ionic conductivity through interface conduction. Our findings demonstrate a promising electrolyte for LT-SOFC applications is on-line produced from initial YSZ-BZY composite electrolyte.

Limitations of the study

The study of these electrolyte materials can be further integrated into a deeper understanding of the composite material's conduction mechanism.

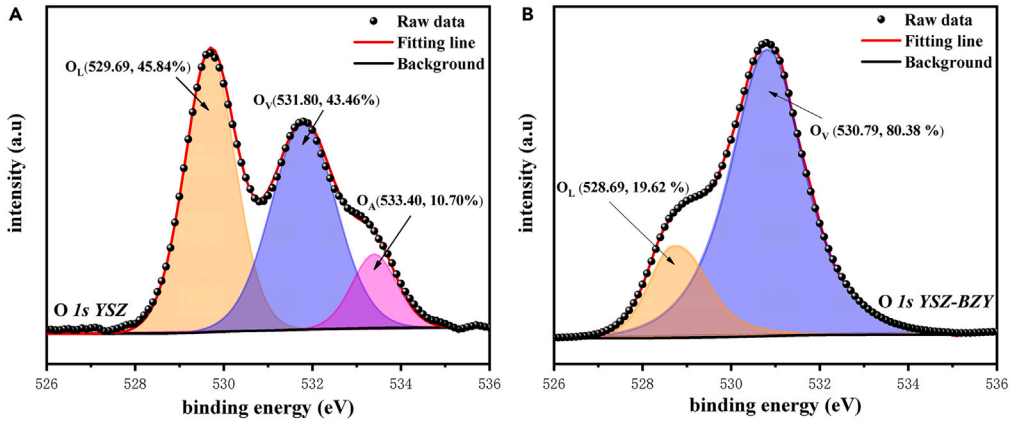

Figure 7. XPS characterization

Curve-fitting result for O 1s from (A) YSZ, and (B) the tested YSZ-BZY electrolyte.

STAR★METHODS

Detailed methods are provided in the online version of this paper and include the following:

- KEY RESOURCES TABLE
- RESOURCE AVAILABILITY
  - Lead contact
  - Materials availability
  - Data and code availability
- EXPERIMENTAL MODEL AND SUBJECT DETAILS
- METHOD DETAILS
  - Material and preparation
  - Material characterization
  - Fuel cell manufacturing and performance test
- QUANTIFICATION AND STATISTICAL ANALYSIS
- ADDITIONAL RESOURCES

ACKNOWLEDGMENTS

The authors would like to acknowledge the financial support from the National Natural Science Foundation of China (Grant No. 51872080), Wuhan Science and Technology Bureau (No. 2020010601012293).

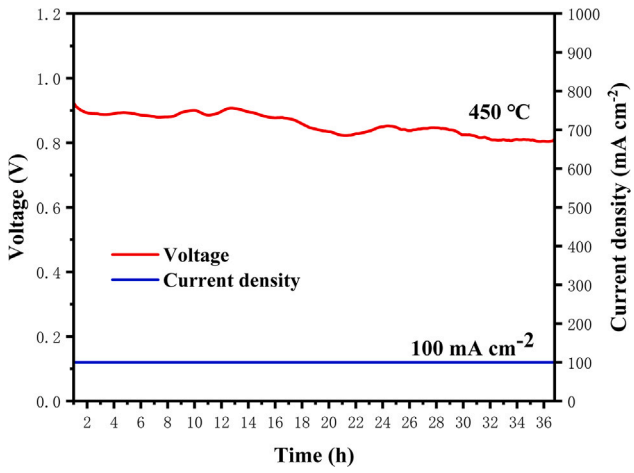

Figure 8. The durability results of YSZ-BZY fuel cell tested at 450°C

AUTHOR CONTRIBUTIONS

Conceptualization, Y.L., B.W., and D.Z.; Data curation, Investigation and Validation, Y.L., C.J., and L.W.; Formal analysis, Methodology, Project administration and Writing – original draft, Y. L.; Supervision, Funding acquisition and Writing – review and editing, D.Z. and B.W. All authors discussed the results. All authors have read and agreed to the published version of the manuscript.

DECLARATION OF INTERESTS

The authors declare no competing interests.

Received: September 27, 2022
Revised: May 2, 2023
Accepted: May 26, 2023
Published: June 1, 2023

REFERENCES

1. Zhu, B., Wang, B., Wang, Y., Raza, R., Tan, W., Kim, J.-S., van Aken, P.A., and Lund, P. (2017). Charge separation and transport in $La_{0.6}Sr_{0.4}Co_{0.2}Fe_{0.8}O_{3-\delta}$ and ion-doping ceria heterostructure material for new generation fuel cell. Nano Energy *37*, 195–202. https://doi.org/10.1016/j.nanoen.2017.05.003.

2. Zhu, B., Lund, P.D., Raza, R., Ma, Y., Fan, L., Afzal, M., Patakangas, J., He, Y., Zhao, Y., Tan, W., et al. (2015). Schottky junction effect on high performance fuel cells based on nanocomposite materials. Adv. Energy Mater. *5*, 1401895. https://doi.org/10.1002/aenm.201401895.

3. Fan, L., Zhu, B., Su, P.-C., and He, C. (2018). Nanomaterials and technologies for low temperature solid oxide fuel cells: recent advances, challenges and opportunities. Nano Energy *45*, 148–176. https://doi.org/10.1016/j.nanoen.2017.12.044.

4. Irshad, M., Siraj, K., Raza, R., Javed, F., Ahsan, M., Shakir, I., and Rafique, M.S. (2016). High performance of SDC and GDC core shell type composite electrolytes using methane as a fuel for low temperature SOFC. AIP Adv. *6*, 025202. https://doi.org/10.1063/1.4941676.

5. Zhu, P., Wang, S., Wang, J., Zhou, L., Shi, P., Xia, C., Afzal, M., Zhang, B., Dong, W., Wang, H., and Lund, P.D. (2016). Novel fuel cell with nanocomposite functional layer designed by perovskite solar cell principle. Nano Energy *1008*, 156–163. https://doi.org/10.1016/j.nanoen.2015.11.015.

6. Wang, B., Wang, Y., Fan, L., Cai, Y., Xia, C., Liu, Y., Raza, R., van Aken, P.A., Wang, H., and zhu, B. (2016). Preparation and characterization of Sm and Ca co-doped ceria–$La_{0.6}Sr_{0.4}Co_{0.2}Fe_{0.8}O_{3-\delta}$ semiconductor-ionic composites for electrolyte-layer-free fuel cells. J. Mater. Chem. A Mater. *4*, 15426–15436. https://doi.org/10.1039/c6ta05763b.

7. Zhu, B., Lund, P.D., Raza, R., Ma, Y., Fan, L., Afzal, M., Patakangas, J., He, Y., Zhao, Y., Tan, W., et al. (2015). Schottky junction effect on high performance fuel cells based on nanocomposite materials. Adv. Energy Mater. *5*, 1401895. https://doi.org/10.1002/aenm.201401895.

8. Zhang, Z., Li, M., Ma, X., Zhou, S.L., Ren, Z.W., and Qiu, Y.S. (2018). In situ formation of a 3D core-shell and triple-conducting oxygen reduction reaction electrode for proton-conducting SOFCs. Chem. Biol. Interact. *296*, 76–82. https://doi.org/10.1016/j.jpowsour.2018.03.029.

9. Cai, Y., Chen, Y., Akbar, M., Jin, B., Tu, Z., Mushtaq, N., Wang, B., Qu, X., Xia, C., and Huang, Y. (2021). A bulk-heterostructure nanocomposite electrolyte of $Ce_{0.8}Sm_{0.2}O_{2-\delta}$-$SrTiO_3$ for low-temperature solid oxide fuel cells. Nano-Micro Lett. *13*, 46. https://doi.org/10.1007/s40820-020-00574-3.

10. Liu, K., Ganesh, K.S., Nie, J., He, Z., Xia, C., Dong, W., Wang, X., Wang, H., and Wang, B. (2020). Characterizing the blocking electron ability of the Schottky junction in SnO_2–SDC semiconductor–ionic membrane fuel cells. ACS Sustain. Chem. Eng. *8*, 10357–10368. https://doi.org/10.1021/acssuschemeng.0c01344.

11. Zhu, B., Mi, Y., Xia, C., Wang, B., Kim, J.-S., Lund, P., and Li, T. (2022). A nanoscale perspective on solid oxide and semiconductor membrane fuel cells: materials and technology. Energy Mater. *1*, 100002. https://doi.org/10.20517/energymater.2021.03.

12. Lu, Y., Zhu, B., Shi, J., and Yun, S. (2022). Advanced low-temperature solid oxide fuel cells based on a built-in electric field. Energy Mater. *1*, 100007. https://doi.org/10.20517/energymater.2021.06.

13. Shah, M.Y., Lu, Y., Mushtaq, N., Singh, M., Rauf, S., Yousaf, M., and Zhu, B. (2022). ZnO/MgZnO heterostructure membrane with type II band alignment for ceramic fuel cells. Energy Mater. *2*, 200031. https://doi.org/10.20517/energymater.2022.27.

14. Deng, H., Feng, C., Zhang, W., Mi, Y., Wang, X., Dong, W., Wang, B., and Zhu, B. (2017). The electrolyte-layer free fuel cell using a semiconductor-ionic $Sr_2Fe_{1.5}Mo_{0.5}O_{6-\delta}$–$Ce_{0.8}Sm_{0.2}O_{2-\delta}$ composite functional membrane. Int. J. Hydrogen Energy *42*, 25001–25007. https://doi.org/10.1016/j.ijhydene.2017.08.113.

15. Zhu, B., Raza, R., Qin, H., Liu, Q., and Fan, L. (2011). Fuel cells based on electrolyte and non-electrolyte separators. Energy Environ. Sci. *4*, 2986. https://doi.org/10.1039/c1ee01202a.

16. Patakangas, J., Ma, Y., Jing, Y., and Lund, P. (2014). Review and analysis of characterization methods and ionic conductivities for low-temperature solid oxide fuel cells (LT-SOFC). J. Power Sources *263*, 315–331. https://doi.org/10.1016/j.jpowsour.2014.04.008.

17. Chen, G., Sun, W., Luo, Y., He, Y., Zhang, X., Zhu, B., Li, W., Liu, X., Ding, Y., Li, Y., et al. (2019). Advanced fuel cell based on new nanocrystalline structure $Gd_{0.1}Ce_{0.9}O_2$ electrolyte. ACS Appl. Mater. Interfaces *11*, 10642–10650. https://doi.org/10.1021/acsami.8b20454.

18. Zhang, W., Cai, Y., Wang, B., Deng, H., Feng, C., Dong, W., Li, J., and Zhu, B. (2016). The fuel cells studies from ionic electrolyte $Ce_{0.8}Sm_{0.05}Ca_{0.15}O_{2-\delta}$ to the mixture layers with semiconductor $Ni_{0.8}Co_{0.15}Al_{0.05}LiO_{2-\delta}$ *41*, 18761–18768. https://doi.org/10.1016/j.ijhydene.2016.01.127.

19. Yuan, M., Dong, W., Wei, L., Liu, Q., Meng, Y., Wang, X., Wang, B., and Zhu, B. (2020). Stability study of SOFC using layered perovskite oxide $La_{1.85}Sr_{0.15}CuO_4$ mixed with ionic conductor as membrane. Electrochim. Acta *332*, 135487. https://doi.org/10.1016/j.electacta.2019.135487.

20. Deng, H., Zhang, W., Wang, X., Mi, Y., Dong, W., Tan, W., and Zhu, B. (2017). An ionic conductor $Ce_{0.8}Sm_{0.2}O_{2-\delta}$ (SDC) and semiconductor $Sm_{0.5}Sr_{0.5}CoO_3$ (SSC) composite for high performance electrolyte-free fuel cell. Int. J. Hydrogen Energy *42*, 22228–22234. https://doi.org/10.1016/j.ijhydene.2017.03.089.

21. Zhu, B., Ma, Y., Wang, X., Raza, R., Qin, H., and Fan, L. (2011). A fuel cell with a single component functioning simultaneously as the electrodes and electrolyte. Electrochem. Commun. *13*, 225–227. https://doi.org/10.1016/j.elecom.2010.12.019.

22. Xia, C., Mi, Y., Wang, B., Lin, B., Chen, G., and Zhu, B. (2019). Shaping triple-conducting

semiconductor $BaCo_{0.4}Fe_{0.4}Zr_{0.1}Y_{0.1}O_{3-\delta}$ into an electrolyte for low-temperature solid oxide fuel cells. Nat. Commun. *10*, 1707. https://doi.org/10.1038/s41467-019-09532-z.

23. Fan, L., Ma, Y., Wang, X., Singh, M., and Zhu, B. (2014). Understanding the electrochemical mechanism of the core–shell ceria–LiZnO nanocomposite in a low temperature solid oxide fuel cell. J. Mater. Chem. A Mater. *2*, 5399. https://doi.org/10.1039/c3ta14098a.

24. Xia, C., Cai, Y., Ma, Y., Wang, B., Zhang, W., Karlsson, M., Wu, Y., and Zhu, B. (2016). Natural mineral-based solid oxide fuel cell with heterogeneous nanocomposite derived from hematite and rare-earth minerals. ACS Appl. Mater. Interfaces *8*, 20748–20755. https://doi.org/10.1021/acsami.6b05694.

25. Feng, C., Wang, B., Zhu, J., Wang, H., and Zhu, B. (2018). Thin-film fuel cells using a sodium silicate binder with $La_{0.6}Sr_{0.4}Co_{0.2}Fe_{0.8}O_{3-\delta}$ (LSCF) and LaCePr oxides (LCP) membranes. Energy Technol. *6*, 312–317. https://doi.org/10.1002/ente.201700469.

26. Magrez, A. (2004). Preparation, sintering, and water incorporation of proton conducting $Ba_{0.99}Zr_{0.8}Y_{0.2}O_{3-\delta}$ comparison between three different synthesis techniques. Solid State Ionics *175*, 585–588. https://doi.org/10.1016/j.ssi.2004.03.045.

27. Li, Y., Gemmen, R., and Liu, X. (2010). Oxygen reduction and transportation mechanisms in solid oxide fuel cell cathodes. J. Power Sources *195*, 3345–3358. https://doi.org/10.1016/j.jpowsour.2009.12.062.

28. Fan, L., Wang, C., Osamudiamen, O., Raza, R., Singh, M., and Zhu, B. (2012). Mixed ion and electron conductive composites for single component fuel cells: I. Effects of composition and pellet thickness. J. Power Sources *217*, 164–169. https://doi.org/10.1016/j.jpowsour.2012.05.045.

29. He, Z., Nie, J., Liu, K., Sivajee Ganesh, K., Akbar, M., Xia, C., Wang, X., Dong, W., Huang, J., and Wang, B. (2021). Compositing protonic conductor $BaZr_{0.5}Y_{0.5}O_3$ (BZY) with triple conductor $BaCo_{0.4}Fe_{0.4}Zr_{0.1}Y_{0.1}O_{3-\delta}$ (BCFZY) as electrolyte for advanced solid oxide fuel cell. Int. J. Hydrogen Energy *46*, 9799–9808. https://doi.org/10.1016/j.ijhydene.2020.06.102.

30. Nuñez, G., Balanay, M.J., and Cervera, R.B.M. (2015). Preparation of Y-doped $BaZrO_3$ proton conducting solid electrolyte via modified low temperature pechini method. Adv. Mater. Res. *1098*, 86–91. https://doi.org/10.4028/www.scientific.net/AMR.1098.86.

31. Giannici, F., Shirpour, M., Longo, A., Martorana, A., Merkle, R., and Maier, J. (2011). Long-range and short-range structure of proton-conducting Y:$BaZrO_3$. Chem. Mater. *23*, 2994–3002. https://doi.org/10.1021/cm200682d.

32. Yang, W., Wang, L., Li, Y., Zhou, H., He, Z., Han, C., and Dai, L. (2021). Properties of Hf doped $BaZr_{0.8}Y_{0.2}O_{3-\delta}$ protonic conductor. Ceram. Int. *47*, 9273–9286. https://doi.org/10.1016/j.ceramint.2020.12.054.

33. Cheng, Z., and Liu, M. (2007). Characterization of sulfur poisoning of Ni–YSZ anodes for solid oxide fuel cells using in situ Raman microspectroscopy. Solid State Ionics *178*, 925–935. https://doi.org/10.1016/j.ssi.2007.04.004.

34. Li, T., Yu, B., Liu, Z., Li, J., Ma, M., Wang, Y., Zhu, M., Yin, H., Wang, X., Fu, Y., et al. (2018). Investigation of interfacial diffusion between YSZ and SNDC through Raman spectroscopy. Nat. Commun. *9*, 11–17. https://doi.org/10.1016/j.ssi.2018.09.008.

35. Strobel, R., Maciejewski, M., Pratsinis, S.E., and Baiker, A. (2006). Unprecedented formation of metastable monoclinic $BaCO_3$ nanoparticles. Thermochim. Acta *445*, 23–26. https://doi.org/10.1016/j.tca.2006.03.020.

36. Wang, Z., Liu, M., Li, X., Blinn, K., Lai, S., Lü, Z., and Liu, M. (2015). Understanding the phase formation and compositions of barium carbonate modified NiO-yttria stabilized zirconia for fuel cell applications. Int. J. Hydrogen Energy *40*, 15597–15604. https://doi.org/10.1016/j.ijhydene.2015.09.092.

37. Chaney, J., Santillán, J.D., Knittle, E., and Williams, Q. (2014). A high-pressure infrared and Raman spectroscopic study of $BaCO_3$: the aragonite, trigonal and Pmmn structures. Phys. Chem. Miner. *42*, 83–93. https://doi.org/10.1007/s00269-014-0702-0.

38. Chen, G., Luo, Y., Sun, W., Liu, H., Ding, Y., Li, Y., Geng, S., Yu, K., and Liu, G. (2018). Electrochemical performance of a new structured low temperature SOFC with BZY electrolyte. Int. J. Hydrogen Energy *43*, 12765–12772. https://doi.org/10.1016/j.ijhydene.2018.04.006.

39. Srinivas Reddy, G., and Bauri, R. (2016). Size-controlled growth of spherical nanoparticles of Y-doped $BaZrO_3$ perovskite. Appl. Phys. A *122*, 428. https://doi.org/10.1007/s00339-016-9982-1.

40. Kesavan, J.K., Luisetto, I., Tuti, S., Meneghini, C., Battocchio, C., and Iucci, G. (2017). Ni supported on YSZ: XAS and XPS characterization and catalytic activity for CO_2 methanation. J. Mater. Sci. *52*, 10331–10340. https://doi.org/10.1007/s10853-017-1179-2.

41. Ntais, S., Isaifan, R.J., and Baranova, E.A. (2014). An X-ray photoelectron spectroscopy study of platinum nanoparticles on yttria-stabilized zirconia ionic support: insight into metal support interaction. Mater. Chem. Phys. *148*, 673–679. https://doi.org/10.1016/j.matchemphys.2014.08.033.

42. Kumari, L., Li, W.Z., Xu, J.M., Leblanc, R.M., Wang, D.Z., Li, Y., Guo, H., and Zhang, J. (2009). Controlled hydrothermal synthesis of zirconium oxide nanostructures and their optical properties. Cryst. Growth Des. *9*, 3874–3880. https://doi.org/10.1021/cg800711m.

STAR★METHODS

KEY RESOURCES TABLE

REAGENT or RESOURCE	SOURCE	IDENTIFIER
Chemicals, peptides, and recombinant proteins		
Terpineol mixture of isomers	Sinopharm Chemical Reagent Co. Ltd.	30173728; CAS: 8000-41-7
Barium nitrate	NanJing Reagent	C0010520223; CAS: 10022-31-8
Yttria-stabilized zirconia	Xiya Reagent	A63148; CAS: 308076-80-4

RESOURCE AVAILABILITY

Lead contact

Further information and requests for resources are accessible from the lead contact, Baoyuan Wang (Email: baoyuanw@163.com)

Materials availability

This study did not generate new unique reagents. The relevant experimental materials described in this paper and any materials prepared in this paper are available.

Data and code availability

- All data reported in this paper will be shared by the lead contact upon request.
- This paper does not report original code.
- Any additional information required to reanalyze the data reported in this paper is available from the lead contact upon request.

EXPERIMENTAL MODEL AND SUBJECT DETAILS

Not relevant to this study.

METHOD DETAILS

Material and preparation

In our study, the $Ba(NO_3)_2$ material was colorless crystal with purity ≥99.0%. The YSZ-$Ba(NO_3)_2$ composite material was prepared using the following procedure: A suitable amount of white barium nitrate ($Ba(NO_3)_2$, 99.0%) crystalline powder was weighed and completely dissolved in deionized water to form barium nitrate aqueous solution. The aforementioned solution was supplemented with 8YSZ (Y_2O_3 8 mol%, 163 m^2/g) powder with a YSZ: $Ba(NO_3)_2$ mass ratio of 45:55, 50:50, 55:45 or 60:40. The mixture was then placed on a magnetic stirrer and stirred for 12 hours at 80°C to create the composite block solid. The two powders were thoroughly combined before being placed in an electric blast drying oven at 120°C for 12 hours, and then placed in the Muffle furnace to calcine for 2 hours at 600°C. After thorough grinding, the homogeneous YSZ-$Ba(NO_3)_2$ composite was produced.

Material characterization

An X-ray diffractometer is used to produce X-ray diffraction (XRD) patterns. Field emission scanning electron microscopy (FESEM) equipped with an Oxford energy-dispersive spectrometer (EDS) was used to examine the samples' surface morphology, element concentration and distribution. The valence states of the elements were examined using X-ray photoelectron spectroscopy (XPS). The Gamry Reference 3000 electrochemical workstation in open-circuit voltage mode, with an ac signal amplitude of 10 mV and frequency range of 1-105 Hz, was used to provide electrochemical impedance spectroscopy (EIS) characterization. The detailed morphology at interface region between two phases was further investigated by high revolution transmission electron microscopy (HR-TEM, JEOL JE-2100F).

Fuel cell manufacturing and performance test

Firstly, the symmetrical electrode pieces were fabricated. In detail, the NCAL slurry was prepared by mixing commercial NCAL powder with terpineol mixture of isomers in a mass ratio of 3:1, and then the slurry was painted evenly with a brush on the nickel foam, finally dried at 110°C for 7-10 minutes to finish the preparation of NCAL electrode pieces. Wherein the nickel foam acts as a current collector, while NCAL is responsible for catalytical reaction. The YSZ-BZY composite powder was sandwiched by two pieces of Ni-NCAL to construct Ni-NCAL/ YSZ-BZY /Ni-NCAL configuration, which was pressed under a loading of 10 MPa for 1-2 minutes to complete fuel cell fabrication. Before the electrochemical performance testing, the cell was pre-treated by H_2 for 1h at 550°C. During the test, ambient air served as the oxidant and hydrogen served as the fuel, and the flow rates of the two kinds of gas were set at 130-150 mL per minute. The current density-voltage (I-V) and current density-power (I-P) curves of the assembled cells were recorded by a computerized instrument (IT8511, ITECH).

QUANTIFICATION AND STATISTICAL ANALYSIS

Our study doesn't include quantification or statistical analysis.

ADDITIONAL RESOURCES

Our study has not generated or contributed to a new website/forum or not been part of a clinical trial.